

ICE MASS CHANGE VERSUS GRAVITY – LOCAL MODELS AND GOCE’S CONTRIBUTION

C. Gisinger¹, F. Heuberger¹, D. Rieser¹, R. Pail², and A. Sharov³

¹Institute of Navigation and Satellite Geodesy, TU Graz, 8010 Graz, Austria

²Institute for Astronomical and Physical Geodesy, TU München, Germany

³Institute of Digital Image Processing, Joanneum Research, 8010 Graz, Austria

ABSTRACT

Ice mass and glacier changes are often observed using geometrical methods. In this paper, a different approach is presented: by investigating the gravitational effects linked to such mass changes, satellite gravity missions like GOCE can be seen as global monitoring instruments for the cryosphere. This work compares synthetic gravity fields of Novaya Zemlya computed by numerical forward modeling to local GOCE solutions based on least squares collocation.

Key words: Forward modeling, GOCE, gravity, cryosphere, least squares collocation.

1. INTRODUCTION

One of the key questions, when investigating the Earth’s gravity field with consideration of climate change, is the sensitivity of space borne gravity missions such as ESA’s Gravity field and steady-state Ocean Circulation Explorer (GOCE) to climate induced mass transports. In the joint project Modeling Snow-Ice cover Evolution and Associated Gravitational Effects with GOCE constraints (ICEAGE), the Institute of Navigation and Satellite Geodesy (INAS), Graz University of Technology, Austria, and the Institute of Digital Image Processing (DIB), Joanneum Research, Austria, are – besides other topics – investigating the interrelation between ice mass change and the regional gravity field in the Eurasian Arctic sector between 31° to 81° East and 73° to 82° North, including Franz-Josefs Land and Northern Novaya Zemlya.

For the investigations presented in this paper, Novaya Zemlya has been selected as principal study region (Fig. 1). The island of Novaya Zemlya is situated between the Kara sea and the Barents sea in northern Russia. There lies the world’s third largest ice sheet of about $22\,000\text{ km}^2$, which qualifies it as a study object for regional ice mass and gravity research, also in the light of current climate change debate.



Figure 1. Novaya Zemlya, the study region in project ICEAGE (Source: Marble).

One way to observe changes of Snow and Ice Resources (SIR) is the derivation of multitemporal geometrical models using space-borne observations from e.g. altimetry and interferometric data from Synthetic Aperture Radar (SAR) missions in combination with topographic maps. By comparison of consecutive geometrical models, changes in the cryosphere and its masses are detectable. Such variations in ice masses can also be seen in changes of the Earth’s gravity field. Thus, a detailed knowledge of the gravity field can deliver valuable information of temporal mass variations in the cryosphere.

To answer the question, whether GOCE might in principle (already) be used to detect ice mass changes at such a small scale, two different approaches are applied: on the one hand, synthetic gravity field solutions computed by numerical forward modeling are based on digital terrain and density models for the test region in order to simulate ice mass variations and their effect on the gravity field. On the other hand, direct mapping of GOCE gradients using least squares collocation (LSC) allows a first glimpse at the unprecedented spatial resolution of GOCE, especially in high latitudes. By comparing the results of these different approaches, a sensitivity analysis for GOCE and (hopefully) follow-on missions is performed.

While an overview of the LSC investigations is given in section 5 as well as in Rieser et al. [2010b], the model setup, methodology and parameter tuning of the numerical forward modeling approach is explained in a more

detailed way in sections 2 and 3. Its research process consists of three parts: part one deals with the model properties

- ice density distribution,
- bedrock topography, and
- ice thickness

to investigate their individual contribution in terms of gravity field changes. In the second part, the temporal variations of the gravity field are simulated based on JR's map of more than half a century's topographic changes of the ice shield in the study region (cf. Pail et al. [2009]). In the case of ice, interior structures and the related changes in density distributions, gravity field variations take place in submilligal range at relatively short wavelengths. Therefore, this type of mass changes is at the edge of being detectable by today's gravity field satellites, as will be shown in the third part, where the synthetic results of numerical forward modeling are compared to a local LSC-solution (GOCE measurements as input observations) in order to give a rough assessment of the satellite's capabilities in detecting such local ice mass variations.

2. NUMERICAL FORWARD MODELING

2.1. Mathematical Background

In case of an arbitrary solid body, its gravity potential V at a certain location P can be described by the well known Newton Integral

$$V = G \iiint_K \frac{1}{l} dm, \quad (1)$$

where G denotes the Newton attraction constant and K is the boundary of the solid body. As shown in Fig. 2, l describes the Euclidean distance between the computation point P and the differential mass element dm which can be substituted by the density-volume relation using the mass element's dimensions (cf. Hofmann-Wellenhof & Moritz [2005]):

$$dm = \rho dv = \rho d\xi d\eta d\zeta. \quad (2)$$

If we transfer the coordinate origin to the computation point P , introduce a density contrast $\Delta\rho$ and assign the x, y, z notation to the differential volume element, Eq. (2) can be rewritten in terms of the disturbing potential T as

$$T = G\Delta\rho \iiint \frac{1}{\sqrt{x^2 + y^2 + z^2}} dx dy dz. \quad (3)$$

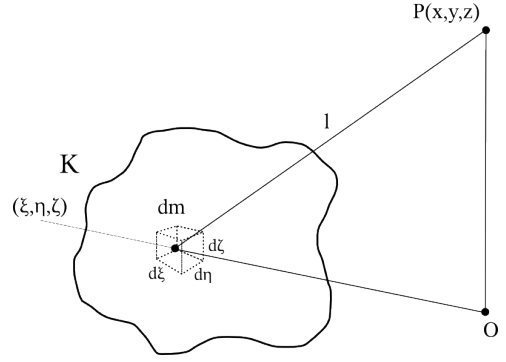


Figure 2. A solid body exerts a gravitational effect which can be quantified at a certain point P by integrating over differential mass elements within the body's boundary K

The first derivative of Eq. (3) with respect to z expresses the gravity anomaly Δg (which is used as gravity field quantity for the results in this research) as

$$\Delta g = -G\Delta\rho \iiint \frac{z}{\sqrt{(x^2 + y^2 + z^2)^3}} dx dy dz. \quad (4)$$

In case of the whole Earth a strict solution for the triple integral would require an analytical representation of the Earth's boundary. Such an analytical description does not exist. Nonetheless, for primitives like prisms or cylinders, a rigorous solution of Eq. (4) is possible. This is the key element of numerical forward modeling, which identifies the single elements of a digital terrain model (DTM) with the boundaries of the triple integral defined for a rectangular prism. Analytical integration yields a closed formula for a prism's gravity effect on an arbitrary defined computation point, practically carried out by using all eight prism corners for the integral solution, as described in Mader [1951]:

$$\Delta g = -G\Delta\rho [x \log(y+r) + y \log(x+r) - z \arctan \frac{xy}{zr}] \Big|_{x1}^{x2} \Big|_{y1}^{y2} \Big|_{z1}^{z2}. \quad (5)$$

By summing up the resulting gravity anomalies Δg of all individual prism elements of the DTM for one particular computation point, the sum yields the model's gravity effect on this point. This whole process is of course well known in remove-restore techniques for gravity field computation (cf. Forsberg [1984]). However, usually a constant density value 2.67 g/cm^3 is applied. In this project, we use a three dimensional density distribution i.e., prisms of different density (Fig. 3) leading to an absolute synthetic gravity field effect instead of terrain reduction. Due to combination of DTM and 3d-density, we speak of a digital terrain density model (DTDM).

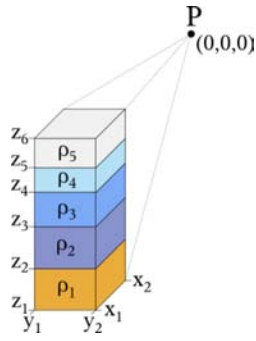


Figure 3. Integration of multiple density prisms yielding their gravitational force acting on the computation point at the origin of a local level frame.

By defining a whole grid of computation points situated on the prism tops or on a constant level above, a synthetic gravity field solution can be calculated representing the gravitational effect of the underlying DTDM, shown in Fig. 4.

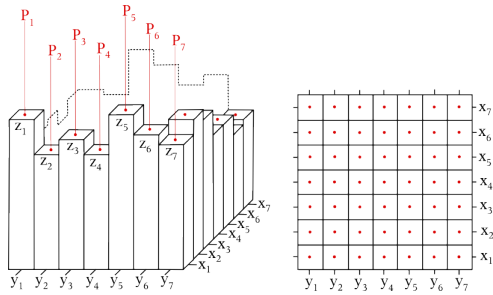


Figure 4. Scheme of a forward modeling situation.

The model itself is defined in a WGS-84 based geographic grid with homogeneous spacing in both directions. In order to meet the requirements of the cartesian coordinate based Eq. (5), a transformation of relevant model parts (mass selection radius 167 km) to a local level frame (North, East, Up) originating at the actual computation point is carried out. This ensures that all the masses are placed correctly during each calculation loop, regarding also the Earth's curvature and the meridian convergence with respect to the computation points.

2.2. Model Composition

As described above, numerical forward modeling relies on the surface geometry and a three-dimensional density distribution. The geometrical representation of Novaya Zemlya is a combination of different data sources: SAR, altimetry and various maps were compiled by JR (cf. Pail et al. [2009]), yielding a digital terrain model of the island itself whereas the International Bathymetric Chart of the Atlantic Ocean (IBCAO) was used for modeling the underwater topography. By merging both DTMS, island DTM and bathymetric data, a detailed geometric model of

Novaya Zemlya and its surroundings could be generated, as can be seen in Fig. 5.

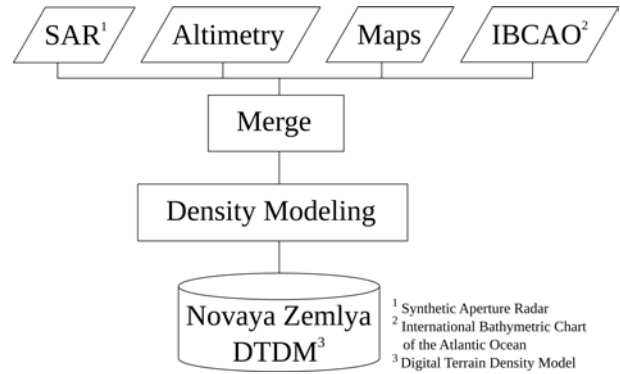


Figure 5. Data flow for the assembly of a digital terrain density model for numerical forward modeling of gravity anomalies in the study region.

The combination of geometry and density information starts with a 3d separation into ice, bedrock and ocean, which are treated individually during the model compilation process. This procedure has several interfaces that can be used to customize the parameters of bedrock and ice regarding both geometry and density in order to simulate different model states. These different models allow the analysis of every individual parameter change in terms of gravity field changes. Due to the primary focus on ice mass change, the densities of bedrock and ocean were set to common constant values, whereas the ice density distribution relies on an empirical depth-density relation described more extensively in section 2.3 and Gisinger et al. [2010].

One example of a final DTDM is shown in Fig. 6, and a close up view is given in Fig. 7.

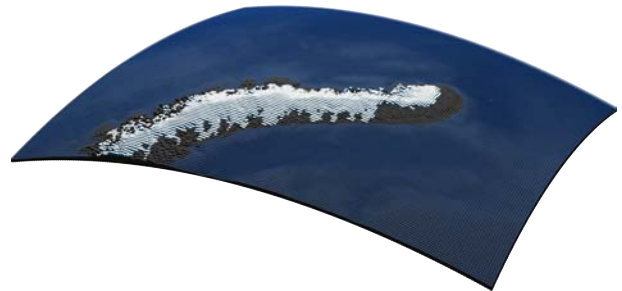


Figure 6. The digital terrain density model of the study region shown as "seen" from a computation point during numerical forward modeling of the gravity anomaly in this point (10 times vertically exaggerated to denote the Earth's curvature).

2.3. Ice Density Modeling

In order to achieve a realistic density distribution within the ice body, the empirical depth-density relation published by Schytt [1956] is used.

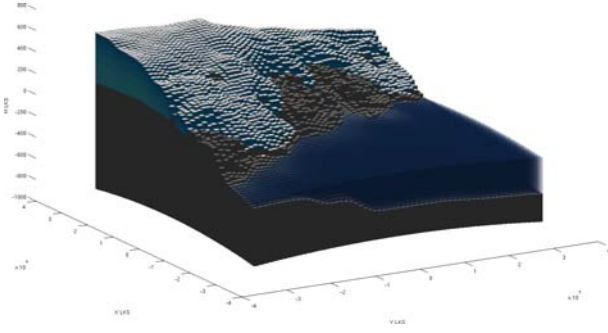


Figure 7. Schematic close-up view of the digital terrain density model, representing different densities for ice (cyan), bedrock (gray) and ocean (blue).

$$\rho(z) = \rho_i - (\rho_i - \rho_s) e^{-Cz} \quad (6)$$

The different parameters were defined in accordance with in situ measurements carried out by JR in 2008: $\rho_i = 917 \text{ kg/m}^3$ is the empirical density of ice, $\rho_s = 550 \text{ kg/m}^3$ is the surface density and $C = 1.9/z_t$ is a site dependent value, governed by the firm-ice transition depth $z_t = 10 \text{ m}$. Fig. 8 shows the resulting depth-density relation function. Quantization into six bins allowed the top down density modeling within the ice prisms as (up to) six layers by means of stapled prisms.

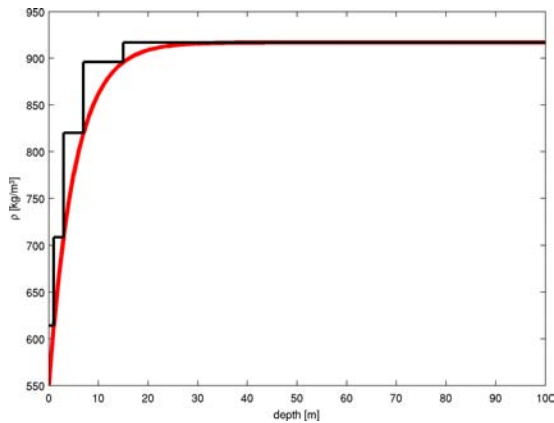


Figure 8. Empirical depth-density relation with Novaya Zemlya parameters (red) and six quantization steps (black).

Due to its low firm-ice transition depth, the model has only a thin hull of lighter SIR and a solid ice core with constant density. This model was compared to a second parametrization in order to determine the impact of different ice densities on the gravity field. Results of this comparison will be demonstrated in the following section.

3. INVESTIGATION OF MODEL PARAMETERS

For every result in this section, the general model setup consists of:

- Spatial resolution of mass model: 0.5 km.
- Computation points at horizontal prism centers, directly on top of the DTM.
- Cross section profile at longitude 65.25° .

All results in this section are gravity anomalies Δg expressed in mgal. To get an impression of the resulting field, Fig. 9 shows the result of the numerical forward modeling process for the DTDM from epoch 2008. In the following paragraphs differences with respect to this “absolute” solution are shown in the course of tuning the model parameters.

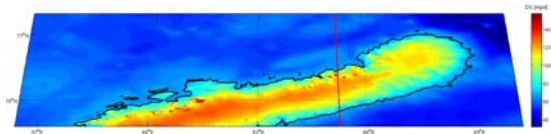


Figure 9. Gravity anomalies (mgal) synthetically computed for epoch 2008 via numerical forward modeling.

3.1. Changes in Ice Geometry

First, we simulated an ice loss of 10% at the main ice shield which would result in a gravity field change in the range of 3 mgal (Fig. 10). This relative ice loss corresponds to about 40 to 50 m at the thickest parts of the ice sheet. It has to be kept in mind that the ice thickness and therefore the underlying bedrock topography are based on the generic lookup table (LUT) described in section 3.2.

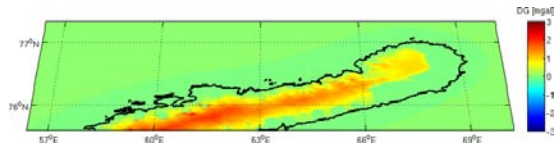


Figure 10. Gravity anomaly differences (mgal) to be expected from an assumed ice mass loss of 10% over the whole study area simulated via numerical forward modeling.

3.2. Bedrock Height

The bedrock height is obtained via a LUT remapping ice heights to surface correlated bedrock topography. Two different LUT settings were compared in Fig. 11 to analyze the consequence of a possible uncertainty in the bedrock height. Both parameter settings are based on

the assumption of parabolic structures as basic form of the ice caps. A closer look at the cross section profile in Fig. 12 shows the interior model changes. The impact on the gravity field solution is caused by a bedrock change of about 50 m at the areas with maximum DTM elevation inside the applied ice mask.

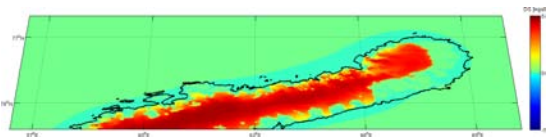


Figure 11. Gravity anomaly differences (mgal) to be expected between different models for the bedrock topography below the ice caps simulated via numerical forward modeling.

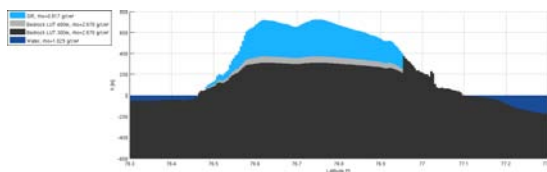


Figure 12. Cross section through the DTDM demonstrating the assumed bedrock uncertainty (gray) resulting in the gravity anomaly differences in Fig. 11.

3.3. Density Model

In Fig. 13, the comparison of gravity fields from two different parameter sets for the ice density confirms the expectation of a small impact (not even 1 mgal). Figs. 14 and 15 show the influence of different firn ice transition depths. Nonetheless, it was decided to keep to the empirically determined local parameters already mentioned in section 2.3.

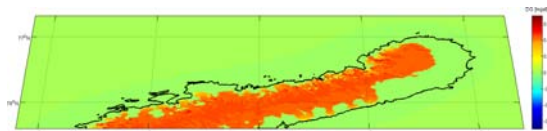


Figure 13. Gravity anomaly differences (mgal) between general Schytt-parameters and "Novaya Zemlya parameters" from section 2.3 simulated via numerical forward modeling.

4. ICE CHANGE DURING THE PAST 60 YEARS

A combination of maps dated around 1950 and present remote sensing data allowed JR the mapping of spatially distributed ice change during the past 60 years. This change map is illustrated in Fig. 16.

The simulation of this geometry variation within our numerical forward modeling framework allows the computation of this surface elevation change interpreted as ice

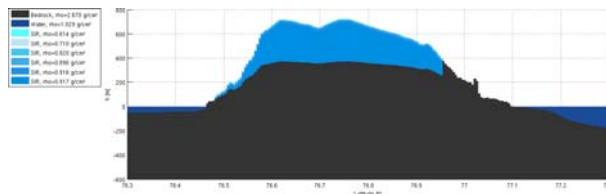


Figure 14. Cross section through the DTDM for the specific Novaya Zemlya parameters for the Schytt model, resulting in six discrete density layers which are barely discernible due to the shallow firn-ice transition depth z_t .

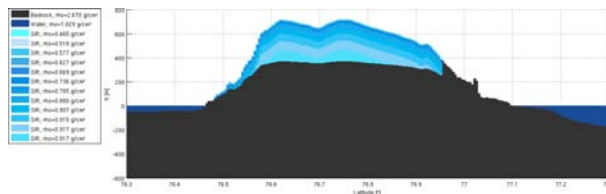


Figure 15. Cross section through the DTDM for general parameters for the Schytt model, resulting in twelve discrete density layers.

mass gain/loss in terms of gravity anomalies. The maximum signal amplitude change of about 6 mgal can be observed at the Northern Ice Cap. This corresponds to about 1 mgal signal variation per decade. Regarding the spatial extent of the Northern Ice Cap's signal change, a region of roughly 800 km² is mainly affected by these significant amplitudes.

Note that the stations for these computations were held at a constant ellipsoidal height of 1500 m. This height (a few hundred meters above the highest point of the used DTDM) was kept in order to avoid misinterpretations due to local gravitational effects acting on computation points directly at the surface of the different DTDMs. Of course, small residuals are still present, based on the neglect of resulting free air corrections, when computation points from two epochs are at a different distances from the actual terrain surface. Additionally, the smaller absolute differences compared to Fig. 10 is also due to the smaller lateral extent of the observed surface changes (opposed to a simulated melting of 10 % over the whole study region).

5. LOCAL GEOID SOLUTIONS

While the numerical forward modeling approach described in the previous sections allows a simulation of gravitational effects based on the topography and also a density distribution in the upper lithosphere with a very high spatial resolution there is neither a way to include global long wavelength information about the gravity field nor a direct validation is possible. Therefore the numerical simulations had to be opposed to local geoid solutions from a different approach. This approach, realized by LSC is described in this section.

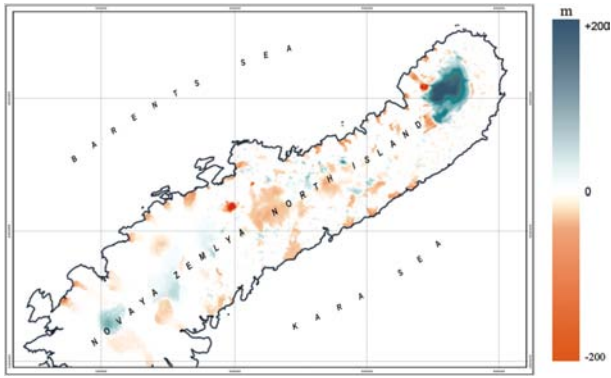


Figure 16. Map of surface elevation changes between the 1950s and 2008 at Novaya Zemlya, compiled by JR.

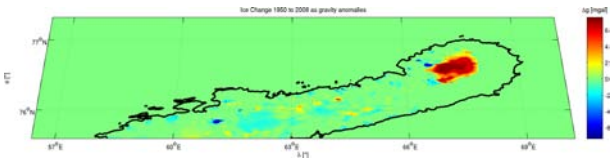


Figure 17. Gravity anomaly differences (mgal) corresponding to the observed surface elevation changes (depicted in Fig. 16) simulated via numerical forward modeling at a constant computation height of 1500 m.

5.1. Least Squares Collocation

LSC allows the usage of GOCE gravity gradients for direct gravity field computation by deriving all necessary quantities from a single covariance model.

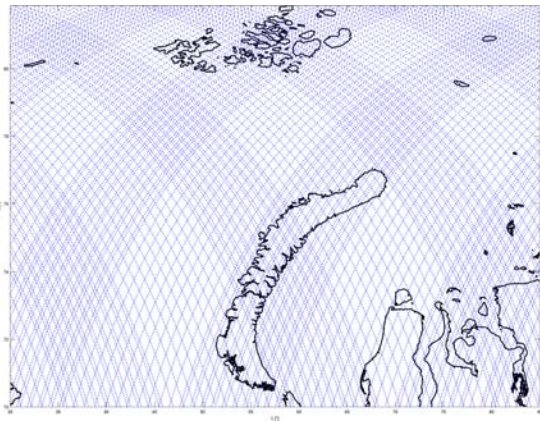


Figure 18. V_{ZZ} gradient tracks from GOCE, November 2009.

In this case, degree variances of Earth Gravity Model 2008 (EGM2008) delivered a global covariance model and Wiener filtering was applied to deal with the colored noise of the gradients. By introducing an adequate stochastic model, the LSC approach yields full stochastic information for a computed solution. Regarding GOCE's data characteristics, the LSC approach has to cope with complex covariance propagation due to frame transfor-

mations between gradiometer reference frame (GRF) and local orbit reference frame (LORF), and the remapping of noisy components of the gravity gradient tensor due to frame rotation. The filtering and transformation processes are described in detail in Rieser et al. [2010a], Rieser & Pail [2009] and Rieser et al. [2010b].

5.2. Preliminary LSC Results

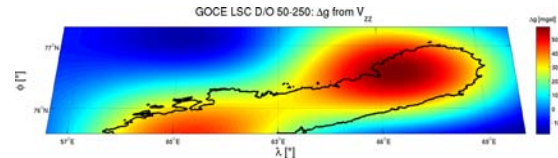


Figure 19. Gravity anomalies (in mgal) from a LSC gravity field solution with GOCE V_{ZZ} gradients from November 2009, corresponding to degrees between 50 and 250.

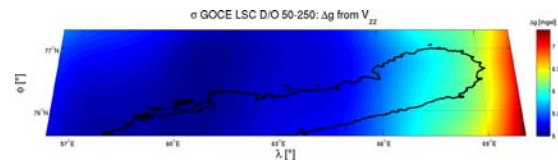


Figure 20. Standard deviations of gravity anomalies (in mgal) from the LSC gravity field solution in Fig. 19

The illustrated gravity field solution (Fig. 19) was computed using solely GOCE vertical gradients from November 2009. As can be seen from the ground track of the used data-set in Fig. 18, the availability of more GOCE observation would certainly improve the solution by removing the edge effect that is easily discernible from the estimated standard deviations in Fig. 20.

6. CONCLUSIONS

6.1. Comparison between synthetic and measured gravity field solutions

Results of the numerical modeling approach described above are not directly comparable to absolute global gravity field solutions: on the one hand, local modeling of mass prisms is mainly based on relative density contrasts in the upper lithosphere. Also, the modeled area is just a finite part of the whole Earth's mass. On the other hand, the high spatial resolution of the used DTM surpasses even high-degree models like solutions from Gravity Recovery and Climate Experiment (GRACE) and GOCE (maximum degree and order up to about 200) or even EGM2008 (maximum degree 2190, cf. Pavlis et al. [2008]).

The comparison of synthetically modeled gravity anomalies Δg (Fig. 21) and LSC solutions from GOCE (Fig. 19) show quite good accordance apart from filter-induced

windowing effects at their common (medium) frequency bandwidth. To allow this (visual) comparison, the high frequency results of the numerical modeling approach had to be low-pass filtered to match the spatial resolution of the GOCE solution corresponding to spherical harmonic degrees between 50 and 250. This was done by applying a two-dimensional Gaussian filter with a kernel size corresponding to about 0.5° and $\sigma = 12$.

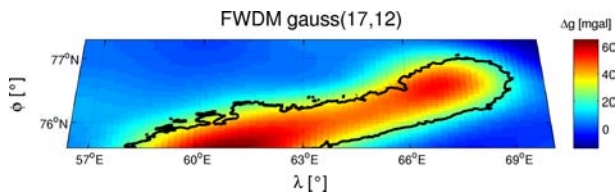


Figure 21. Low-pass filtered gravity solution (gravity anomalies Δg in mgal) computed by numerical forward modeling. Gaussian filter radius corresponding to about 0.5° , $\sigma = 12$.

6.2. Outlook

Looking at the estimated standard deviations from the LSC approach from section 5, the direct application of GOCE gradients shows encouraging results already for short time-series at such a high spatial resolution, by nearly reaching the predicted 1 mgal accuracy for a narrow grid of computation points (about 5 km). Nevertheless, the simulated effects of ice mass change can not yet fully be detected by GOCE. This will change if longer time-series or – even better – multitemporal gravity field solutions become achievable thanks to GOCE's performance and (hopefully) future satellite gravity missions.

ACKNOWLEDGMENTS

The project ICEAGE was performed in the frame of the Austrian Space Application Programme (ASAP), Phase 5, funded by the Austrian Research Promotion Agency (FFG), project number 817106.

REFERENCES

- Forsberg, R. 1984, A study of terrain reductions, density anomalies and geophysical inversion methods in gravity field modelling, Tech. Rep. 355, The Ohio State University, Columbus
- Gisinger, C., Heuberger, F., Rieser, D., Pail, R., & Sharov, A. 2010, Numerical forward modeling of gravity signals caused by glacier mass changes in Novaya Zemlya, Poster presented at the 2010 General Assembly of the European Geosciences Union, Vienna

- Hofmann-Wellenhof, B. & Moritz, H. 2005, Physical Geodesy (Springer, Wien, New, York)
- Mader, K. 1951, Österreichische Zeitschrift für Vermessungswesen, Österreichischer Verein für Vermessungswesen, Sonderheft 11
- Pail, R., Sharov, A., Rieser, D., Heuberger, F., & Gisinger, C. 2009, Modelling snow-ice cover evolution and associated gravitational effects with GOCE constraints (ICEAGE), Midterm Report, technical report, FFG, Austrian Space Applications Programme
- Pavlis, N. K., Holmes, S., Kenyon, S., & Factor, J. 2008, An Earth Gravitational Model to Degree 2160: EGM2008, Poster presented at the 2008 General Assembly of the European Geosciences Union, Vienna
- Rieser, D., Gisinger, C., Heuberger, F., Pail, R., & Sharov, A. 2010a, Spatial correlation between the Earth's gravity field and glacier change signals in the Eurasian Arctic, Poster presented at the 2010 General Assembly of the European Geosciences Union, Vienna
- Rieser, D. & Pail, R. 2009, Using GOCE Gravity Gradients For A Combined Regional Gravity Field Solution With Least Squares Collocation, Poster presented at the IAG 2010, Buenos Aires
- Rieser, D., Pail, R., & Sharov, A. 2010b, in Refining Regional Gravity Field Solutions with Goce Gravity Gradients for Cryospheric Investigations, Living Planet Symposium Conference Proceedings, ESA, submitted
- Schytt, V. 1956, in Report on glaciological investigations during the Norwegian-British-Swedish Antarctic Expedition, 1949-1952, Summary of the glaciological work, Assn. Intern. Hydrologic, Vol. 4, IUGG, Rome, 236–243